

Enhanced strain-rate sensitivity in f.c.c. nanocrystals due to grain-boundary diffusion and sliding

Yujie Wei, Allan F. Bower[†], Huajian Gao^{*}

Division of Engineering, Brown University, Providence RI 02912, U.S.A.

Abstract: Recent experiments on f.c.c. and h.c.p. nanocrystalline metals reported an increase of more than ten fold in strain-rate sensitivity in contrast to their conventional coarse-grained counterparts. To improve our understanding of this issue, we consider a mesoscopic continuum model of a two-dimensional polycrystal with deformation mechanisms including grain interior plasticity, grain-boundary diffusion and grain-boundary sliding. The model captures the transition from sliding and diffusion dominated creep in nanocrystals with relatively small grain sizes at low strain rates to plasticity dominated flow in nanocrystals with larger grain sizes at higher strain rates. The strain-rate sensitivity obtained from our calculations matches well with the experimental data for nanocrystalline Cu. Based on this analysis, an analytical model incorporating the competition between grain interior plasticity and grain boundary deformation mechanisms is proposed to provide an intuitive understanding of the transition in strain-rate sensitivity in nanostructured metals.

Keywords: nanocrystalline materials; strain-rate sensitivity; grain-boundary diffusion; grain-boundary sliding; grain-interior plasticity

1. Introduction

It has long been observed that the flow stress of most metals increases when the materials are subjected to higher loading rates, e.g. [1-3]. The variation of flow stress σ with strain rate $\dot{\epsilon}$ in uniaxial tension is usually characterized by a strain-rate exponent $m = \partial \ln \sigma / \partial \ln \dot{\epsilon}$, which can be interpreted as the slope of a graph of $\log(\sigma)$ as a function of $\log(\dot{\epsilon})$. In many materials, the strain rate exponent is constant over a wide range of strain rates, in which case the stress is related to the strain rate by a simple power law

$$\sigma = \sigma_0 \left(\frac{\dot{\epsilon}}{\dot{\epsilon}_0} \right)^m \quad (1)$$

where σ_0 is the flow stress at the strain rate of $\dot{\epsilon}_0$.

corresponding author:

[†]Allan Bower: allan_bower@brown.edu; ^{*}Huajian Gao: huajian_gao@brown.edu.

Recent experiments on f.c.c. and h.c.p. nanocrystalline (nc) metals reported a more than ten fold increase in strain-rate sensitivity m in contrast to their conventional coarse-grained counterparts. For example, values of the strain-rate exponent m measured in several tests on polycrystalline copper are plotted as a function of grain size d in Fig. 1. These data suggest that, while the stress exponent m is only around 0.01 for grain size exceeding 1 micron, it increases quickly for grain size below 100nm, reaches $m=0.25$ for $d=26\text{nm}$, and can even approach $m=1$ for small grains in the strain rate regime of $\dot{\epsilon} < 10^{-7} / \text{s}$ [4].

A number of explanations have been proposed for these observations. By assuming that dislocation activities are the rate-controlling plastic deformation in nc materials, Cheng et al. [4] related the activation volume of thermally assisted plastic deformation to both dislocation density and grain size. In smaller grains, they obtained a lower activation volume. Based on the theory of Conrad [1] that strain rate sensitivity is proportional to the reciprocal of activation volume, the model by Cheng et al. [5] could explain the enhanced m with decreasing grain size. A model based on the concept of dislocation density cannot be applied to materials with grain sizes below a few tens of nanometers, since plastic flow in these materials occurs primarily by the emission of complete or partial dislocations in grain boundaries [6-8]. Asaro and Suresh [9] developed models that can be used to estimate the activation volume associated with these dislocation emission-absorption processes. Their calculations also led to estimates of activation volumes becoming lower in smaller grains, which is consistent with the increase in strain-rate sensitivity with decreasing grain size observed in f.c.c. nanocrystalline materials.

Alternatively, the variation of strain-rate sensitivity with grain size can be explained in terms of deformation mechanisms associated with the grain boundaries themselves. It is known that grain-boundary (GB) sliding and diffusion provide substantial contributions to plastic strain rates in polycrystalline materials at high temperatures. For example, GB diffusion plays a critical role in controlling stress relaxation in thin polycrystalline films [10-11]. It has also been observed that constrained GB diffusion can lead to novel dislocation mechanisms [12-15] and induce transient stress concentration [16]. Gleiter [17] suggested nearly two decades ago that GB diffusion may play a dominant role in nc materials even at the room temperature. Gleiter's argument was based on the Coble creep rate [18] for a polycrystalline solid

$$\dot{\epsilon} = \alpha \frac{\delta D \Omega}{k T} \frac{\sigma}{d^3} \quad (4)$$

where d is the grain size, Ω the atomic volume, δ is the thickness of the layer in which grain boundary diffusion is assumed to take place, D the GB diffusivity and α a constant. This expression shows that the Coble creep rate is expected to become more important as the grain size decreases. Although GB diffusion has never been directly observed experimentally, there is strong indirect evidence, both experimental and computational, that GB diffusion plays an important role in nc materials. For example, Yamakov et al. [19] performed molecular dynamics simulations that showed that Coble-creep plays a dominate role in nc Palladium. Lu et al. [20] attributed their observations of super-extensible nc Cu strips at the room temperature to GB diffusion. Jiang et al. [4] conducted experiments on nc Cu

synthesized by electric brush plating with $d \approx 30\text{nm}$ and reported a strong dependence of rate sensitivity exponent on strain rate even at room temperature, a behavior which can be interpreted as a transition in deformation mechanism to GB diffusion or GB sliding at low strain rates. It is likely that both dislocation motion and GB deformation mechanisms, including GB diffusion and GB sliding, play important roles in controlling rate sensitivity of nc materials. Along this line, several models have been developed. For example, Zhu et al. [21] extended the polycrystal plasticity framework of Asaro and Needleman [22] to incorporate GB sliding and account for grain size dependence of dislocation flow. Their model was used to predict the influence of grain size and grain size distribution on the effective properties of nc materials. This approach was extended further by Wei and Gao [23] to account for deformation by GB diffusion, together with a more rigorous description of plastic deformation by dislocation emission-absorption mechanisms. This model predicted a substantial increase in strain-rate sensitivity m as the dominant plastic deformation mechanisms shifts from grain interior to GBs.

Although the previous models included both grain interior and GB mechanisms that contribute to plastic flow, their predictions are often based on mean-field approximations to the distribution of stress and strain in the polycrystal. Such an approach effectively assumes that the deformations in GBs and grain interiors operate independently. In reality, however, GB sliding or GB diffusion cannot operate independently in the absence of some other mechanism of deformation. This leads to a strong coupling between the deformation mechanisms that cannot be easily incorporated into a mean-field theory.

In this paper, we intend to develop a more rigorous model of deformation in nc materials that accounts for the coupling between GB processes and dislocation activity within the grains. We idealize a representative polycrystal as an assembly of grains separated by sharp GBs, as shown in Fig. 2. The GBs act as fast diffusion paths, and also permit adjacent grains to slide relative to one another. Deformation in the interior of a grain is modeled by single crystal plasticity. The increase in flow strength of the grains with reducing grain size is modeled phenomenologically, by making the resistance of individual slip systems a function of the size of each grain. Simple arguments based on dislocation mechanics are used to construct appropriate relationships between grain size and slip resistance.

Our model is similar in some respects to several mesoscopic models developed to study the deformation of nanostructured materials (e.g., Schwaiger et al. [24], and Fu [25]). In these models, the GBs were approximated as layers of finite thickness which undergo rate-independent plastic deformation but have dissimilar properties to the bulk of the grain. Wei and Anand [26], Warner et al. [27] and Jérusalem et al. [28] used sharp interface models to account for the effects of GB sliding and separation, where GB sliding was assumed to be rate independent. Wei et al. [29] later developed a rate-dependent amorphous model for the GB region to study the strain-rate sensitivity, GB shearing failure and GB cavitation in nanostructured materials. None of these models accounted for the effects of GB diffusion. The goal of this work is to study the role of GB sliding and diffusion in controlling strain rate sensitivity of nc materials with different grain sizes.

The remainder of this paper is organized as follows. We will describe the modeling method in Section 2 and apply this method to study the deformation of nc Cu in Section 3. A macroscopic constitutive model on strain-rate sensitivity is presented in Section 4 to supply an intuitive understanding on the competition between grain interiors and grain-boundaries at different grain sizes and strain rates. Some discussion and conclusion statements are made in Section 5.

2. Modeling

A polycrystal is modeled as a two dimensional assembly of elastic-viscoplastic grains separated by sharp GBs. The polycrystal is subjected to plane strain deformation with macroscopic strains no more than 3% in our calculations. Deformation in the grain interior is modeled with anisotropic single crystal plasticity. The crystal can also deform plastically by stress driven mass transport along the GBs, as well as by GB sliding. The reader is referred to Bower and Wininger [30] for a detailed description of a more general formulation for modeling migration, diffusion, sliding of GBs as well as plastic deformation in grain interiors. The governing equations for GB diffusion and sliding, as well as grain interior plasticity are briefly discussed here.

- **Grain-boundary diffusion**

Grain boundaries serve as fast diffusion paths for vacancy (atoms) migration, driven by a non-uniform chemical potential along the GB. As illustrated in Fig. 2a, at a point x along the GB, the chemical potential at x is given as [31]

$$\mu = \mu_0 - \Omega \sigma_n \quad (5)$$

where σ_n denotes the normal traction at x and μ_0 is a reference potential in the stress-free state, taken to be zero in the present study. The Nernst-Einstein equation for atomic flux j is

$$j = - \frac{\delta D}{k T \Omega} \frac{\partial \mu}{\partial x} \quad (6)$$

Mass conservation requires that the rate of material accumulation at x is related to the divergence of volumetric flux as

$$\frac{\partial u_n}{\partial t} = - \frac{\partial(\Omega j)}{\partial x} = - \frac{\delta D \Omega}{k T} \frac{\partial^2 \sigma_n}{\partial x^2} \quad (7)$$

where t is time and $u_n = (\mathbf{u}^+ - \mathbf{u}^-) \cdot \mathbf{n}$ is the width of new material being inserted at x by GB diffusion. For subsequent calculations, it is helpful to normalize Eqn. (7) as

$$\frac{\partial \bar{u}_n}{\partial \bar{t}} = - \frac{\partial^2 \bar{\sigma}_n}{\partial \bar{x}^2} \quad (8)$$

where $\bar{u}_n = u_n / d$, $\bar{x} = x / d$, $\bar{t} = t / t_0$, $\bar{\sigma}_n = \sigma_n / E^*$, d being the averaged grain size, E^* the plane strain modulus and t_0 a characteristic time defined as

$$t_0 = \frac{kT d^3}{\delta D \Omega E^*} \quad (9)$$

- **Grain-boundary sliding**

In response to local shear stress on a GB, two neighboring grains adhering via the GB can slide with respect to each other. We adopt a Newtonian viscous law to describe the shearing resistance and relative sliding velocity,

$$\xi \frac{\partial u_s}{\partial t} = \tau_s \quad (10)$$

where $u_s = (\mathbf{u}^+ - \mathbf{u}^-) \cdot \mathbf{m}$ is the relative sliding displacement across the GB in response to the shear traction τ_s (Fig. 2a) and ξ is the GB viscosity. Eqn. (10) can be normalized as

$$\frac{\partial \bar{u}_s}{\partial \bar{t}} = \bar{\eta} \bar{\tau}_s, \quad \text{with} \quad \bar{\eta} = \frac{kT d^2}{\delta D \Omega \xi}, \quad (11)$$

where $\bar{u}_s = u_s / d$, $\bar{t} = t / t_0$, $\bar{\tau}_s = \tau_s / E^*$. The non-dimensional parameter $\bar{\eta}$, hereafter referred to as the grain-boundary fluidity, provides a relative measure of the creep rate induced by GB sliding compared to that by GB diffusion.

It is important to note that neither GB sliding nor GB diffusion can occur in a solid unless some other mechanism of deformation can accommodate the resulting incompatible velocity discontinuity across the GB [29-30]. In the creep literature, it is common to describe various processes involving GB sliding as different mechanisms [32]; for example, sliding accommodated by dislocation creep has been commonly referred to as Rachinger sliding [33], while sliding accommodated by diffusion has been referred to as Lifshitz sliding [34]. In addition, elastic deformation of grain interior could also accommodate parts of GB sliding [29]. In our framework, we do not distinguish explicitly among these processes. The coupling between GB sliding, diffusion, and grain interior mechanisms emerges naturally as a consequence of enforcing compatibility and equilibrium on the overall deformation by means of the finite element method.

The influence of normal traction on GB sliding is neglected in the present work. Molecular dynamics simulations by Bringa et al. [35] on nanocrystalline Cu showed that the flow stress of grain boundaries can be sensitive to normal pressure. Several constitutive models have also discussed the pressure dependence of GB sliding and GB cavitation by means of a simple Mohr-Coulomb criterion [26, 29, 36]. A summary of different modeling strategies on GB sliding in nanocrystalline regime has been provided in the review article by Meyers et al. [37]. In principle, we can also include such pressure dependence by adding a term $\mu\sigma$ to the

left side of Eqn (10). However, it is difficult to determine accurate values for the pressure sensitivity, and it is not clear that behavior observed in the extreme strain rates and applied stresses typical in molecular dynamic simulations accurately characterizes behavior under creep conditions.

- **Triple junction**

In a microstructure composed of multiple grains, a junction of three or more grains is usually a site of high stress concentration, where cavitation or other forms of damage could be initiated, due to severely mismatched properties of adjacent grains and/or GBs. In the limited scope of this paper, no damage or GB decohesion will be considered. GB junctions serve as bridges for atoms to transfer between interconnected boundaries. Mass conservation in the junction requires the sum of fluxes from all GBs meeting at one junction to be zero. Strong constraints are imposed in our numerical implementation to ensure mass conservation and chemical potential continuity at any internal GB junctions.

- **Grain interior plasticity**

As pointed out by Wei and Anand [26], a standard crystal plasticity model for the grain-interior deformation, which implicitly assumes enough dislocation nucleation and multiplication events for a sufficiently smooth macroscopic response, is inadequate to represent the limited amount of inelastic deformation due to emission and eventual absorption of the relatively few (partial or complete) dislocations from GBs in nc materials. However, since elastic anisotropy is still important in nc materials, and since the few dislocations in these materials are still expected to move on slip systems, the mathematical structure of continuum crystal plasticity is still useful as an indicator of the limited inelasticity due to crystalline slip within the nc grains. We employ the classical framework of rate-dependent single-crystal plasticity, e.g., [22, 38-39], to model grain-interior plasticity. In such framework, the total strain rate $\dot{\epsilon}_{ij}$ is decomposed into elastic ($\dot{\epsilon}_{ij}^e$) and plastic ($\dot{\gamma}_{ij}$) parts as

$$\dot{\epsilon}_{ij} = \dot{\epsilon}_{ij}^e + \dot{\gamma}_{ij} \quad (12)$$

The elastic strain rate $\dot{\epsilon}_{ij}^e$ is related to the stress rate by the usual linear elastic constitutive equation

$$\dot{\sigma}_{ij} = C_{ijkl} \dot{\epsilon}_{kl}^e \quad (13)$$

where $\dot{\sigma}_{ij}$ are the increment of stress components σ_{ij} from one time step to the next and C_{ijkl} is the fourth order elasticity tensor.

Plastic flow takes place through slip on prescribed crystallographic slip systems, with each system α defined by a slip direction \mathbf{S}^α and a slip-plane normal \mathbf{m}^α . The total plastic strain rate $\dot{\gamma}_{ij}$ is

$$\dot{\gamma}_{ij} = \sum_{\alpha} \dot{\gamma}_{ij}^{\alpha} = \sum_{\alpha} \dot{\gamma}^{\alpha} \frac{s_i^{\alpha} m_j^{\alpha} + s_j^{\alpha} m_i^{\alpha}}{2} \quad (14)$$

where $\dot{\gamma}^{\alpha}$ is the shearing rate on the α -th slip system.

In materials with grain size less than 50 nm, dislocations (full or partial) emitted from GBs play a dominant role in plastic flow. For an approximate phenomenological description of size-dependent plastic flow in the grain interiors, the plastic slip rate on each slip system can be calculated using the rate-dependent law suggested by Asaro and Needleman [22] as

$$\dot{\gamma}^{\alpha} = \dot{\gamma}_0 \left(\frac{|\tau^{\alpha}|}{\tau_c} \right)^{1/\bar{m}} \text{sign}(\tau^{\alpha}) \quad (15)$$

where $\dot{\gamma}_0$ and \bar{m} denote a reference strain rate and strain-rate sensitivity associated with dislocation motion; τ^{α} is the resolved shear stress on the α -th slip system and $\tau_c(d)$ is the slip resistance to complete dislocations in a grain with size d . The grain size dependence of $\tau_c(d)$ is believed to arise mainly from the increasing resistance to nucleation of dislocation loops as the grain size decreases. If full dislocations are emitted from GBs, we follow Zhu et al. [21] in assuming that the dependence of the slip resistance on grain size can be approximately described as

$$\tau_c = \frac{Gb}{d} \quad (16)$$

The resolved shear stress τ^{α} is related to the local stress field σ_{ij} as

$$\tau^{\alpha} = s_i^{\alpha} \sigma_{ij} m_j^{\alpha}$$

As the grain size is reduced to a value comparable to the spacing between partial dislocations, plastic flow occurs as a result of partial dislocations emitted from GBs [7, 9]. In this case, the slip resistance will be expressed as [21, 26]

$$\tau_p = \frac{Gb}{3d} \quad (17)$$

Since each partial dislocation is trailed by a stacking fault with energy γ_{sf} , a threshold stress of $\tau_{th} = \gamma_{sf}/b_p$ is required to ‘initiate’ plastic flow due to partial dislocations, b_p being the

Burgers vector of a partial dislocation. Plastic slip rate due to partial dislocations could be therefore written as:

$$\dot{\gamma}^\alpha = \begin{cases} \dot{\gamma}_0 \left[\frac{(\tau^\alpha - \tau_{th})}{\tau_p} \right]^{1/\bar{m}} & \text{if } \tau^\alpha > \tau_{th} \\ 0 & \text{otherwise} \end{cases} \quad (18)$$

Equating Eqn. (16) to the sum of Eqn. (17) and the threshold stress, i.e., $\tau_c = \tau_p + \tau_{th}$, we can deduce a critical grain size d_c for a transition from plastic flow accommodated by full dislocations to that by partial dislocations as [21, 40]

$$d_c = \frac{2Gbb_p}{3\gamma_{sf}} \quad (19)$$

While full dislocations move along $\langle 01\bar{1} \rangle (111)$ slip systems for f.c.c. metals, partial dislocations move along $\langle \bar{2}11 \rangle (111)$ faulting systems [17, 21] when $d < d_c$.

We have implemented the above constitutive models for GB diffusion, GB sliding, and grain-interior plasticity in finite element software Abaqus [41] to simulate the mechanical behavior of polycrystalline aggregates. This method is applied to investigate the mechanical behavior of nc copper in the next section.

3. Application to nanocrystalline Copper

Nanocrystalline Cu is chosen as a model case for the application of our modeling methodology introduced in the previous section. Specifically, highly rate-sensitive tensile stress-strain curves reported by Jiang et al. [4] (Fig. 3a) are adopted to calibrate the material parameters in the constitutive equations. We use the two-dimensional microstructure in Fig. 2b to represent a nanocrystalline aggregate. Grain sizes in the microstructure roughly follow a lognormal distribution.

The first step is to estimate material parameters in constitutive models discussed in Section 2, including physical constants and material parameters needed for GB diffusion, $\{k, T, d, \delta D, \Omega, E\}$ in Eqn. (7) or (9), viscosity to GB sliding $\{\xi\}$ in Eqn. (11), equivalently $\{\bar{\eta}\}$ in dimensionless form, anisotropic elastic constants C_{ijkl} in Eqn. (13), parameters for plastic slip rates $\{\dot{\gamma}_0, \bar{m}\}$ in Eqn. (15) and material properties $\{G, b, b_p, \gamma_{sf}\}$ in Eqn. (19).

To model nc Cu (with $d \approx 30\text{nm}$) tested by Jiang et al. [4] at room temperature ($T=300$), we need suitable values for GB diffusivity $\{\delta D\}$, GB viscosity $\{\xi\}$ or equivalently $\{\bar{\eta}\}$, and parameters for plastic slip rates $\{\dot{\gamma}_0, \bar{m}\}$. We restrict our attention to strain-rate effects induced by GB deformation mechanisms. Plastic flow in the grain interior is taken to be

nearly rate independent by assigning a small value to $\bar{m} = 0.005$. The reference slip rate in nanocrystals controlled by dislocation emission from GBs is expressed as [23]

$$\dot{\gamma}_0 = \beta^* \nu_d \exp\left(-\frac{\Delta G}{kT}\right) \quad (20)$$

where β^* is a geometrical factor on the order of 1, ν_d the Debye frequency, and ΔG the activation energy for dislocation emission. The Debye frequency is about $\nu_d \approx 10^{13}/s$ [42]. Considering that dislocation emission involves vacancy formation in a GB region [43], we let ΔG be approximated by the vacancy-formation energy of Cu, which is $1.17 \pm 0.11 eV$ [44]. Taking $\beta^* = 1$, we obtain $\dot{\gamma}_0 \approx 10^{-7}/s$. Since we have no information about the relative significance of deformation by diffusion and sliding in GBs, we further assume that these two mechanisms are locally comparable so that $\bar{\eta} = 1$. The GB diffusivity is obtained by fitting the stress-strain curve to the experimental data at a strain-rate of $\dot{\epsilon} = 10^{-6}/s$ in Fig. 3a. The fitted GB diffusivity is $\delta D = 9 \times 10^{-30} m^3/s$, about two orders of magnitude faster than that for conventional coarse-grained polycrystalline Cu [45], which is consistent with the experimental observation of enhanced diffusivity in nc materials [46].

All material parameters used to model the collective mechanical behavior in nc Cu with grain-interior plasticity, GB diffusion and GB sliding, are listed below.

- Elastic constants for single crystal Cu: $C_{11} = 170 \text{ GPa}$, $C_{12} = 120 \text{ GPa}$, and $C_{44} = 75 \text{ GPa}$ [47].
- Stacking fault energy $\gamma_{sf} = 45 \text{ mJ/m}^2$ [48].
- Atomic volume $\Omega = 1.18 \times 10^{-29} m^3$; the Burgers vector for complete and partial dislocations in Cu are $b = 0.256 \text{ nm}$ and $b_p = 0.148 \text{ nm}$ respectively.
- Isotropic elastic constants for Cu: $E = 135 \text{ GPa}$, $G = 40 \text{ GPa}$.
- Critical grain size $d_c = 18 \text{ nm}$; averaged grain size $d = 30 \text{ nm}$.
- Temperature: $T = 300 \text{ K}$.
- Material parameters for plastic slip rates: $\dot{\gamma}_0 = 10^{-7}/s$, $\bar{m} = 0.005$
- GB diffusivity: $\delta D = 9 \times 10^{-30} m^3/s$
- GB fluidity: $\bar{\eta} = 1$

With these material parameters, we perform simulations to investigate the deformation transition in a nanocrystal Cu sample with $d = 30 \text{ nm}$ at different strain rates. The macroscopic stress-strain curves (computed from the relative displacement of the boundaries of the specimen, and the resultant forces applied to the boundaries) are given in Fig. 3b. The macroscopic stress-strain behavior from our model matches quantitatively well with the experimental stress-strain curves in Fig. 3a. The difference in the elastic modulus between the experimental data and our simulation results may be induced by the machine compliance during the experiments. Another possibility is that the lower modulus could be associated with deformation resulting from pre-existing defects like porosity in real materials.

Next we check the role played by individual deformation mechanisms when the sample is deformed at different strain rates, in order to understand the controlling mechanisms for strain-rate sensitivity. The strain rates contributed by GB sliding, diffusion and grain interior plasticity at different strain rates are calculated respectively as following:

$$\dot{\epsilon}_{ij}^{gbs} = \frac{1}{V} \int_{\Gamma} \frac{(\Delta \mathbf{u}^+ - \Delta \mathbf{u}^-) \cdot \mathbf{m}}{\Delta t} \frac{(n_i m_j + m_i n_j)}{2} ds \quad (21a)$$

$$\dot{\epsilon}_{ij}^{gbd} = \frac{1}{V} \int_{\Gamma} \frac{(\Delta \mathbf{u}^+ - \Delta \mathbf{u}^-) \cdot \mathbf{n}}{\Delta t} n_i n_j ds \quad (21b)$$

$$\dot{\epsilon}_{ij}^{gip} = \frac{1}{V} \int_V \sum_{\alpha} \dot{\gamma}^{\alpha} \frac{(s_i^{\alpha} m_j^{\alpha} + m_i^{\alpha} s_j^{\alpha})}{2} dV \quad (21c)$$

where $\Delta \mathbf{u}$ in Eqns. (22a) and (22b) is a displacement increment in a GB from one time step to the next with a span of Δt , V is the volume of the sample and Γ is the total grain-boundary network. The superscript ‘*gbd*’, ‘*gbs*’, and ‘*gip*’ refer to strain rates (hereafter referred to as “mechanism strain rates”) due to GB diffusion, GB sliding, and grain interior plasticity respectively. Fig. 4 shows the evolution of mechanism strain fractions (the respective normal component along the loading axis) with strain rates. The strain fraction of each deformation mechanism is taken at a total applied strain of 1.5%. Plastic deformation shifts from GB to grain interiors as strain rates increases. At a strain rate $< 10^{-5}/s$, plastic deformation is mainly accommodated by GB diffusion and sliding; as the strain rate exceeds $1/s$, grain interior plasticity is the primary contributor for inelastic deformation. Note that the behavior we reported here is based on the assumption that GB deformation is governed by thermally assisted diffusion and viscous sliding. At extremely high rates of strain, such as those typical of molecular dynamic simulations, diffusion and viscous sliding cannot fully occur during the time-scale of the simulation. Under these conditions, deformation in GBs is governed by athermal sliding and separation, which is beyond the scopes of this work.

Fig. 5a shows the strain-rate sensitivity m versus strain-rates for nc Cu from the experiments by Jiang et al. [4] and that based on our calculations. The model predictions are in excellent agreement with experiment. In both theory and experiment, the strain-rate sensitivity m increases quickly when the strain rate is below $10^{-5}/s$ in nc Cu of $d=30nm$, indicating a shift of deformation behavior from grain interiors to GBs. This is consistent with the change in the fraction contributed to the total strain rate by the three deformation mechanisms (diffusion, sliding, and plasticity) shown in Fig. 4. Note that plastic deformation fractions contributed by relatively large grains through full dislocation emission and that by small grains with partial dislocation mechanism are plotted separately. Small grains essentially serve as hard particles and contribute almost no plasticity. Fig. 5b shows the flow stress at different grain size versus strain rates from both modeling and experiments. A transition from diffusion and sliding controlled steady-state flow stress at low strain rates to that determined by plastic deformation in grains is clearly seen. At the low end of strain rates, there is a linear

relationship between strain rates and flow stresses. Toward the high end of strain rates, flow stresses become saturated at strengths controlled by plastic deformation in the grain interior.

The transition from sliding and diffusion dominated flow at low strain rates to grain interior dominated plasticity in the nc aggregates with fixed average grain size can also be illustrated by plotting contours of an equivalent plastic strain in the grains, which is defined as

$$\bar{\varepsilon}^p = \int \dot{\varepsilon}^p dt \quad \text{where} \quad \dot{\varepsilon}^p = \sqrt{(2/3) \dot{\varepsilon}_{ij}^{gip} \dot{\varepsilon}_{ij}^{gip}}$$

The contours of equivalent plastic strain $\bar{\varepsilon}^p$ in grain interior at different strain rates are shown in Fig. 6. The snapshots are taken at a total strain of 1.5% at all strain rates. As strain rate increases, plastic deformation shows three typical types of behavior: (i) at a strain rate $< 10^{-6}$ /s, plastic deformation is accommodated by GB diffusion and sliding alone, Fig. 6a; (ii) at a strain rate between 10^{-6} /s and 10^{-4} /s, Figs. 6b and 6c, plastic deformation comes from both GB region and grain interiors; (iii) grain interior plastic deformation becomes dominant with shear band type of plastic deformation for strain rates $> 10^{-2}$ /s, Figs. 6d-6f.

The deformation behavior for the microstructure with an average grain size 20nm and 50nm has also been studied. Figs 7a and 7b give the stress-strain curves for these two microstructures at several strain-rates. The stress-strain curves seem to converge when the applied strain-rate is high enough, indicating that GB deformation is negligible under that circumstance. Since creep rate by GB diffusion and sliding is expected to be fifteen fold faster in the 20nm sample than that in the 50nm sample, GB deformation dominates around $\dot{\varepsilon} = 10^{-6}$ /s in the former and around $\dot{\varepsilon} = 10^{-7}$ /s in the latter. The equivalent plastic strain snapshots in grain interiors are shown in Figs. 7c-7f, which are taken at a total strain of 1.5% for all strain rates. For $d=20$ nm at $\dot{\varepsilon} = 10^{-5}$ /s, GB deformation contributes the most to the overall plastic deformation (Fig. 7c), and grain interior plasticity starts to take over when $\dot{\varepsilon} = 10^{-3}$ /s.

For the $d=50$ nm sample, grain interior plasticity contributes a significant fraction to the overall plasticity at $\dot{\varepsilon} = 10^{-5}$ /s and becomes dominant at $\dot{\varepsilon} = 10^{-3}$ /s. The stress-strain curves for different grain sizes at a given strain rate of $\dot{\varepsilon} = 10^{-4}$ /s show a transition of the flow stress as the grain size decreases, see Fig. 8.

Note that Fig. 8 shows that the flow stress at a fixed strain rate of 10^{-4} /s first increases with decreasing grain sizes, reaches a peak at $d=20$ nm and then decreases. The increase in strength is due to enhanced resistance to plastic flow in the grain interiors. In contrast, the resistance to diffusion and sliding decreases as the grain size is reduced, and eventually this effect dominates. The grain size corresponding to the maximum flow stress decreases with increased strain rate: this behavior can be understood from a simple analytical model discussed in the next section.

4. Macroscopic constitutive model of strain-rate sensitivity

The strain-rate sensitivity behavior from our model can be approximated by a macroscopic constitutive model. Let ϕ_{gb} be the strain-rate fraction contributed by GB diffusion and GB sliding. We consolidate these two GB mechanisms into one term since the creep rates contributed by them have a linear dependence on stress. The grain interior plasticity mechanism contributes a strain-rate fraction of ϕ_{dp} from all grains smaller than d_c , and ϕ_{dc} from all grains bigger than d_c . We expect

$$\phi_{gb} + f\phi_{dc} + (1-f)\phi_{dp} = 1 \quad (22)$$

to hold at steady-state creep, where f is the volume fraction of grains larger than d_c . To get the volume fraction f , for simplicity we assume that the grain size distribution $p(x)$ follows a Rayleigh distribution instead of the well-known log-normal distribution, i.e.,

$$p(x) = \frac{x}{d_0^2} \exp\left(-\frac{x^2}{2d_0^2}\right) \quad (23)$$

Such a one parameter distribution gives an average grain size of $d = \sqrt{\pi/2} d_0$. The volume fraction f of grains larger than d_c can be expressed as

$$f = 1 - \operatorname{erf}\left(\frac{d_c}{\sqrt{2} d_0}\right) \quad \text{with} \quad \operatorname{erf}(x) = \frac{2}{\sqrt{\pi}} \int_0^x \exp(-x^2) dx \quad (24)$$

The corresponding average grain sizes in the region of $d > d_c$ and $d < d_c$ are defined respectively as

$$\tilde{d} = \frac{\int_{d_c}^{\infty} x p(x) dx}{\int_{d_c}^{\infty} p(x) dx} \quad \text{and} \quad \bar{d} = \frac{\int_0^{d_c} x p(x) dx}{\int_0^{d_c} p(x) dx}, \quad (25)$$

or

$$\tilde{d} = \sqrt{\frac{\pi}{2}} d_0 \left[1 - \operatorname{erf}\left(\frac{d_c}{\sqrt{2} d_0}\right) \right] \exp\left(\frac{d_c^2}{2d_0^2}\right) + d_c \quad (26a)$$

$$\bar{d} = \left\{ \sqrt{\frac{\pi}{2}} d_0 \operatorname{erf}\left(\frac{d_c}{\sqrt{2} d_0}\right) - d_c \exp\left(-\frac{d_c^2}{2d_0^2}\right) \right\} / \left[1 - \exp\left(-\frac{d_c^2}{2d_0^2}\right) \right] \quad (26b)$$

We will use \tilde{d} and \bar{d} to calculate the ‘representative slip resistance’ to full (τ_c) and partial (τ_p) dislocations in our macroscopic model using Eqn. (16) and Eqn. (17). At a strain rate of $\dot{\epsilon}$, the strain-rate fractions ϕ_{gb} , ϕ_{dc} and ϕ_{dp} are defined respectively as

$$\phi_{gb} = \alpha \frac{\delta D \Omega}{k T} \frac{\sigma}{d^3} \frac{1}{\dot{\epsilon}} \quad (27a)$$

$$\phi_{dc} = \frac{\dot{\gamma}_0}{\dot{\epsilon}} \left(\frac{\sigma}{2\tau_c} \right)^{1/\bar{m}} \quad (27b)$$

$$\phi_{dp} = \frac{\dot{\gamma}_0}{\dot{\epsilon}} \left(\frac{\sigma - 2\tau_{th}}{2\tau_p} \right)^{1/\bar{m}} \quad \text{if } \sigma > 2\tau_{th} \quad (27c)$$

Note that we have assumed in Eqns (27b) and (27c) that a polycrystal with representative slip resistance τ has a macroscopic strength of 2τ . Substituting Eqns. (16-17) and (26-27) into Eqn. (22), we can obtain the flow stress under a given strain rate $\dot{\epsilon}$ by solving the nonlinear equation using the Newton-Raphson method. Further, with $m = \partial \ln \sigma / \partial \ln \dot{\epsilon}$, strain-rate sensitivity m at any given strain rate is obtained. The coefficient α in Eqn. (17b) is on the order of unity when the GB fluidity $\bar{\eta}$ is equal to 1 [29] and is taken to be 1 in the following discussion.

Fig. 9 shows the dependence of strain-rate m on both grain sizes (Fig. 9a) and loading rates (Fig. 9b) predicted by this model. The strain-rate sensitivity m increases quickly for strain rates below a grain-size dependent critical value, indicating a shift of deformation behavior from grain interiors to GBs. Fig. 9c shows the steady-state flow stress vs. strain rate for different grain sizes. The trends of strain rate fractions under different strain rates for several grain sizes are shown in Fig. 9d. The simple model depicts the dependence of m on grain sizes and loading rates qualitatively well.

The predicted influence of strain-rate sensitivity \bar{m} in grains on the deformation in GBs, grain-interior plasticity by full dislocations and that by partial dislocations is shown in Fig. 10. The average grain size is chosen to be 20nm so that a large number of grains are below the transitional grain size d_c . The strain-rate fraction by GB mechanisms (including both diffusion and sliding) is 1 at extremely low strain rates and zero at sufficiently high strain rates; for intermediate strain rates, it decreases with increasing strain rates. Increasing \bar{m} slightly speeds up the transition. The contribution from grain interior plasticity via partial dislocation is negligible in the low strain rate regime, and becomes significant in the high strain rate regime as \bar{m} increases. For large \bar{m} , partial dislocations will dominate the plastic deformation in grain interiors. Blue curves are the strain-rate fraction of grain interior plasticity via complete dislocations at different \bar{m} . It increases monotonically with increasing strain rates when \bar{m} is close to zero. For relatively large \bar{m} , its contribution increases with strain rates in the low strain rate regime, reaches a maximum and then starts to decrease at further increase of strain rates. Note that the observed transition from grain

interior plasticity via complete dislocations to that via partial dislocations at high strain rates relies on two factors: (i) the grain size is so distributed that the volume fractions of grains bigger and smaller than d_c are comparable; (ii) there is a high strain rate dependence of the dislocation mechanisms in grain interior plasticity. Although we have assumed GB is the only rate-sensitive mechanism in Section 3 and the results match quantitatively well with experimental observations, it is an outcome of our assumptions but not a proof that dislocation accommodated grain interior deformation is rate-independent. Indeed, the dislocation emission-absorption process could be rate dependent. Our analysis indicates that there may be a transition between partial and complete dislocation activities when grain interior plasticity is rate dependent.

5. Conclusion and discussion

In this paper, we have investigated the deformation behavior of nc materials where GB diffusion and GB sliding play an important role. We have considered the time dependent deformation processes associated with mass-transport along GBs and sliding between neighbouring GBs in response to GB shear traction, while applying single-crystal plasticity to model dislocation motion in the grain interiors. Even though dislocations are not explicitly modeled, the influence of grain size on plastic flow in the grain interior is incorporated using phenomenological constitutive equations based on dislocation motion in a confined environment.

Our model suggests that the experimentally observed variations of strain rate sensitivity with strain rates and grain size can be quantitatively explained by a transition from sliding and diffusion dominated creep in nanocrystals with relatively small grain sizes deformed at low strain rates to plasticity dominated flow in nanocrystals with larger grain size at higher strain rates. The strain-rate sensitivity obtained from our calculations matches well with the reported experimental data. Our results show that the increase in strain rate sensitivity at reduced grain sizes in f.c.c. and h.c.p. nanocrystalline materials can be attributed to a transition from dislocation dominated plasticity to creep under combined GB diffusion and sliding. A simple model of the strain-rate sensitivity has been adopted to provide an intuitive understanding of the competing deformation mechanisms between grain interior plasticity and GB creep.

Plasticity models alone are inadequate to describe the limited amount of inelastic deformation due to emission and absorption of a few (partial or complete) dislocations from GBs in nc materials. In our constitutive equations for GB diffusion and sliding, the relationships between GB stress and GB velocity are independent of plastic deformation in grain interiors. In practice, this may not be the case - for example, it is well known that, as dislocations impinge on GBs, they may be absorbed, giving rise to additional GB sliding and migration. Ashby [43] pointed out that vacancies (or atoms) can only be removed or added to a boundary at the site of GB dislocations, which in turn complicates the diffusion and sliding process. Indeed, Artz et al. [49] and Cocks [50] analyzed the macroscopic creep behavior in

polycrystalline solids in which interface reaction is involved, and the creep behavior is essentially nonlinear in that circumstance.

The dislocation activities in grain interior (e.g., emission-absorption at GBs) can influence GB diffusion and sliding in a number of ways, and GB diffusion in turn can induce local stress concentration and aid dislocation emission. The intricate coupling between grain interior plasticity and GB creep cannot be completely modeled with local constitutive equations. Developing more sophisticated non-local constitutive models capable of capturing the interaction between grain interior slip and GB diffusion/sliding should be a promising area for future study.

Acknowledgment

The research reported is partially supported by the NSF MRSEC at program (award no. DMR-0520651) at Brown University. This support is gratefully acknowledged.

References

- [1] Conrad H. The cryogenic properties of metals. In: Zackay, V.F., editor, High strength materials, John Wiley and Sons, Inc., New York; 1965. p. 436.
- [2] Johnson GR, Cook WH. Engineering Fracture Mechanics 1985;21:31.
- [3] Meyers MF, Dynamic Behavior of Materials, John-Wiley & Sons, Inc., New York, 1994. p. 323.
- [4] Jiang ZH, Liu XL, Li GY, Jang Q, Lian JS, Appl. Phys. Lett. 2006;88:143115.
- [5] Cheng S, Ma E, Wang YM, Kecskes LJ, Youssef KM, Koch CC, Trociowitz UP, Han K, Acta Mater. 2005;53:1521.
- [6] Schiotz J, Tolla FDD, Jacobsen KW, Nature 1998;391:561.
- [7] Wolf D, Yamakov V, hillpot SR, Mukherjee A, Gleiter H, Acta Mater. 2005;53:1.
- [8] Van Swygenhoven H, Derlet PM, Froseth AG, Acta Mater. 2006;54:1975.
- [9] Asaro RJ, Suresh S, Acta Mater. 2005;53:3369.
- [10] Thouless M D, Rodbell KP, Cabral Jr C, J. Vac. Sci. Tech - Vacuum, Surfaces, and Films 1996;14:2454.
- [11] Kobrinsky MJ, Thompson CV, Appl. Phys. Lett. 1998;73:2429.
- [12] Gao HJ, Zhang L, Nix WD, Thompson CV, Arzt E, Acta Mater. 1999;47:2865.
- [13] Balk TJ, Dehm G, Arzt E, Acta Mat. 2003;51:4471.
- [14] Buehler MJ, Hartmaier A, Gao HJ, J of the Mech. Phys. Solids 2003;51:2105.

- [15] Hartmaier A, Buehler MJ, Gao HJ, *Adv. Engng. Mat.* 2005;7:1.
- [16] Wei YJ, Bower AF, Gao HJ, *J. Mech. Phys. Solids*, 2007; in press, doi: 10.1016/j.jmps.2007.08.007.
- [17] Gleiter H, *Prog. Mater. Sci.* 1989;33:223.
- [18] Coble RL, *J. of Applied Physics* 1963;34:1679.
- [19] Yamakov V, Wolf D, Phillpot SR, Gleiter H, *Acta Mater.* 2002;50:61.
- [20] Lu L, Sui ML, Lu K, *Science* 2000;287:1463.
- [21] Zhu B, Asaro RJ, Krysl P, Bailey R, *Acta Mater.* 2005;53:4825.
- [22] Asaro RJ, Needleman A. *Acta Metallurgica* 1985;33:923.
- [23] Wei YJ, Gao HJ, *Materials Science and Engineering A* 2007; in press.
- [24] Schwaiger R, Moser B, Dao M, Chollacoop N, Suresh S, *Acta Mater.* 2003;51:5159.
- [25] Fu HH, Benson DJ, Meyers MA, *Acta Mater.* 2004;52:4413.
- [26] Wei YJ, Anand L, *J of the Mech. Phys. Solids* 2004;52:2587.
- [27] Warner DH, Sansoz F, Molinari JF, *Int J of Plasticity* 2006;22:754.
- [28] Jérusalem A, Stainier L, Radovitzky R, *Phil. Mag.* 2007;87:2541.
- [29] Wei YJ, Su C, Anand L, *Acta Materialia*, 2006;54:3177.
- [30] Bower AF, Wininger E, *J. Mech. Phys. Solids* 2004;52:1289.
- [31] Herring C, *J. of Applied Physics* 1950;21:437.
- [32] Langdon T J, *J. Mater. Sci.* 2006;41:597.
- [33] Rachinger WA, *J. Inst. Metals.* 1952;81:33.
- [34] Lifshitz IM, *Sov. Phys. JETP.* 1963;17:909.
- [35] Bringa EM, Caro A, Wang YM, Victoria M, McNaney JM, Remington BA, Smith RF, Torralva BR, Van Swygenhoven H, *Science* 2005;309:1838.
- [36] Lebensohn RA, Bringa EM, Caro A, *Acta Mat.* 2007;55:261.
- [37] Meyers MA, Mishra A, Benson DJ. *Prog Mater Sci* 2006;51:427.
- [38] Kalidindi SR, Bronkhorst CA, Anand L. *J Mech. Phys. Solids* 1992;40:537.
- [39] Bronkhorst CA, Kalidindi SR, Anand L. *Phil Tran.. Roy Soc. London A* 1992;341:443.
- [40] Asaro RJ, Krysl, P, Kad B, *Phil Mag Lett* 2003;83:733.
- [41] *Abaqus Reference Manuals*, 2006, Simuli Inc., Pawtucket, R.I.
- [42] Reed-Hill RE, *Physical Metallurgy Principles*, 1964. Princeton, N.J., Van Nostrand.
- [43] Ashby MF, *Surf. Sci.* 1972;31:498.
- [44] Simmons RO, Balluffi RW, *Phys. Rev.* 1963;129:1533.
- [45] Frost H, Ashby MF, *Deformation Mechanism Maps: the plasticity and creep of metals and ceramic*, Pergamon Press, Oxford, 1982.
- [46] Wurschum R, Herth S, Brossmann U., *Adv. Eng. Mat.* 2003;5:365.

- [47] Simmons G, Wang H, Single crystal elastic constants and calculated aggregate properties. The MIT Press, Cambridge, 1971.
- [48] Hirth JP, Lothe J, Theory of Dislocations, Wiley, New York, ed. 2, 1982.
- [49] Arzt E, Ashby MF, Verrall RA, Acta Metall. 1983;31:1977.
- [50] Cocks ACF, Mechanics of Materials 1992;13:165.
- [51] Carreker RP, Hibbard WR, Acta Metall. 1953;1: 656.
- [52] Elmustata AA, Tambwe MF, Stone DS, MRS Symp. Proc. 2003;750:Y.8.14.1.
- [53] Gray GT, Lowe TC, Cady CM, Valiev RZ, Aleksandrov IV, Nanostruct. Mater. 1997;9:477.
- [54] Lu L, Li SX, Lu K, Scripta Mater. 2001;45:1163.
- [55] Lu L, Schwaiger R, Shan ZW, Dao M, Lu K, Suresh S, Acta Mater. 2005;53:2169.
- [56] Valiev RZ, Alexandrov OV, Zhu YT, Lowe TC, J. Mater. Res. 2002;17:5.
- [57] Wang YM, Ma E, Mater. Trans. JIM 2003;44:1926.
- [58] Wang YM, Ma E, Acta Mater. 2004;52:1699.
- [59] Wei Q, Cheng S, Ramesh KT, Ma E, Mater. Sci. Eng. A 2004;381:71.

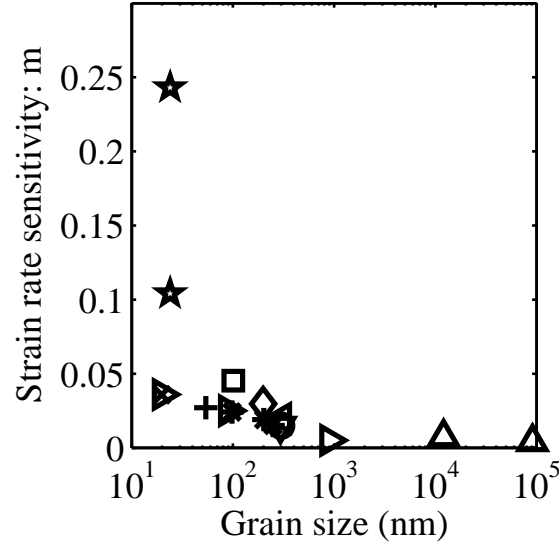
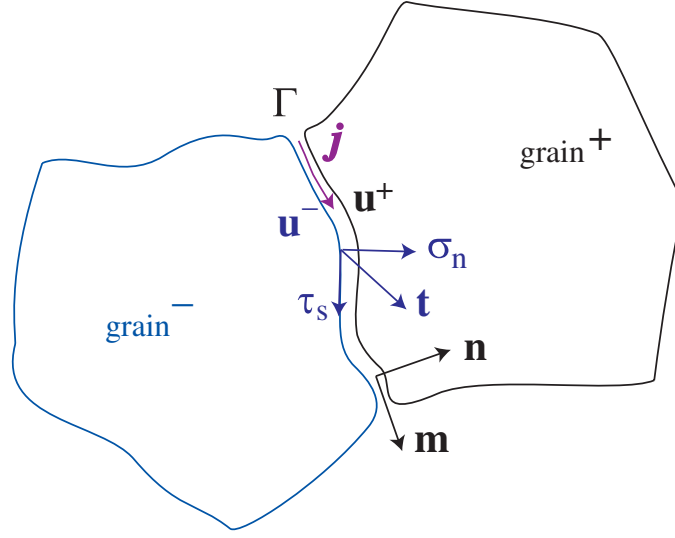
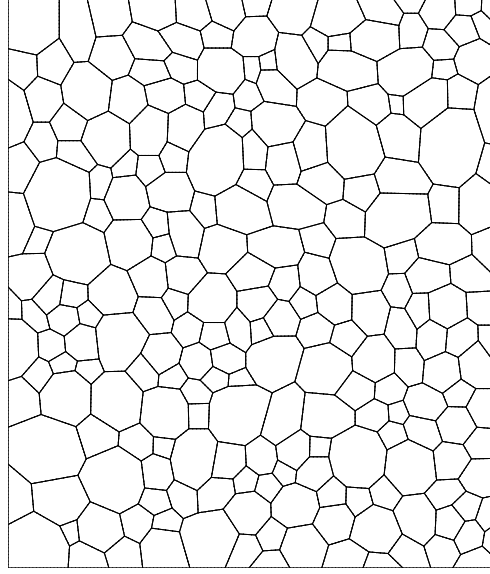


Fig. 1. Compiled data on strain-rate sensitivity m in polycrystalline Copper with different grain sizes. An enhanced strain-rate sensitivity of more than ten folds is observed as the grain size changes from tens of microns to about 20nm. Here m is defined as $m = \partial \ln \sigma / \partial \ln \dot{\epsilon}$ for σ being the uniaxial flow stress and $\dot{\epsilon}$ being the applied strain rate. \triangle (Carreker et al. [51]); $+$ (Cheng et al. [4]); \triangleleft (Elmustata et al. [52]); \circ (Gray et al. [53]); \times (Lu et al. [54]); \triangleright (Lu et al. [55]); \square (Valiev et al. [56]); \diamond (Wang et al. [57]); ∇ (Wang et al. [58]); $*$ (Wei et al. [59]); \star (Jiang et al. [20]).

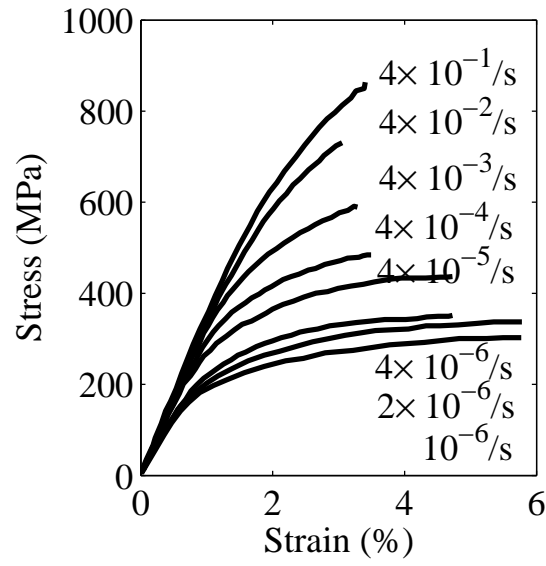


(a)

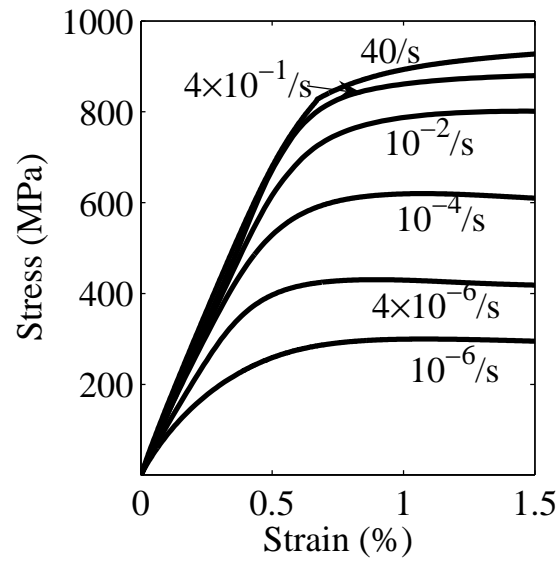


(b)

Fig. 2. Two dimensional model of a polycrystalline solid. (a) A representative GB (Γ) with atomic flux (\mathbf{j}), displacements \mathbf{u}^- and \mathbf{u}^+ across the boundary, normal (\mathbf{n}) and tangential (\mathbf{m}) directions, as well as normal (σ_n) and shear (τ_s) tractions. (b) The two dimensional polycrystalline aggregate adopted in our study.



(a)



(b)

Fig. 3. Stress-strain curves for nc Cu with an average grain size of about 30nm. (a) Reported stress-strain curves in simple tension for different strain-rates from experiments by Jiang et al. [15]; (b) predictions from our model.

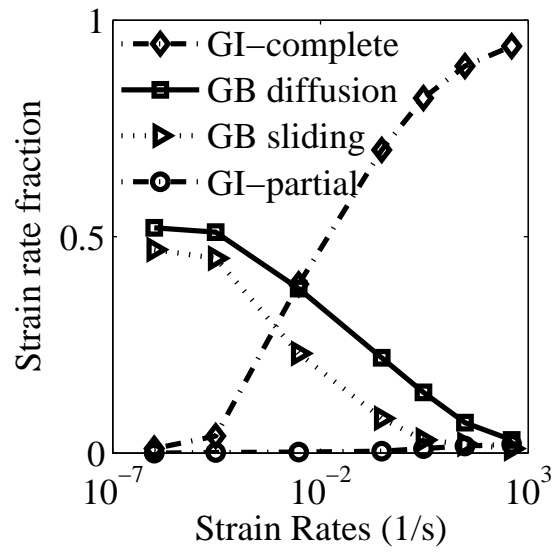


Fig. 4. Mechanism strain rate fractions (at a total applied strain of 1.5%) as a function of the macroscopic strain-rate for a polycrystal with an average grain size of 30nm. At increasing strain rates, plastic deformation is seen to shift from GB creep mechanisms to grain interior plasticity (contributed by motion of complete dislocations in relatively large grains and that of partial dislocations in very small grains). For strain rates below 10^{-5} /s, plastic deformation is primarily accommodated by GB diffusion and sliding. For strain rates larger than 1/s, grain interior deformation becomes dominant.

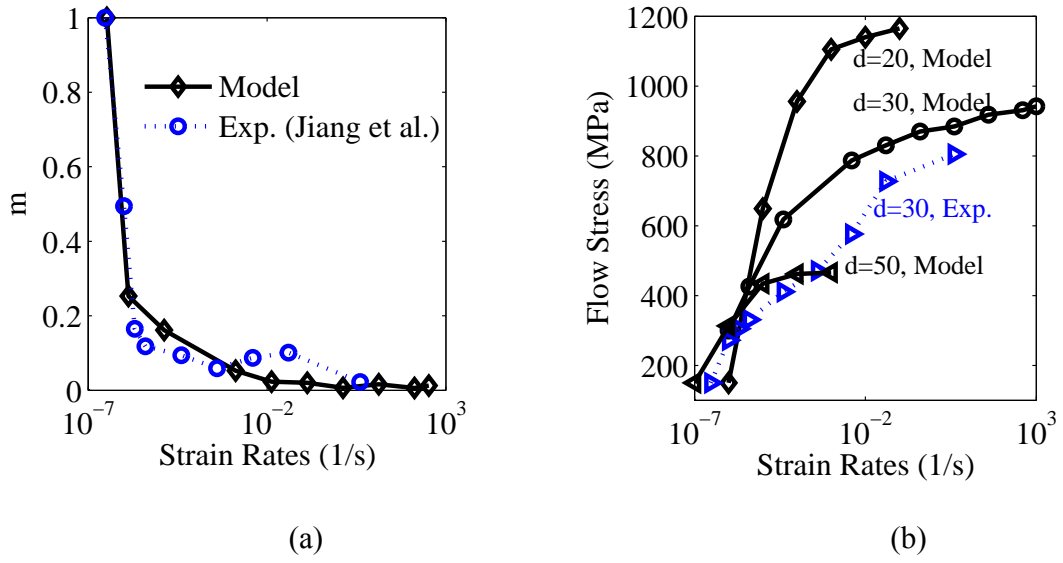


Fig. 5. Strain-rate sensitivity in nc Cu from both experiments by Jiang et al. [15] and the present model. (a) In nc Cu with an average grain size of $d=30\text{nm}$, the strain-rate sensitivity m increases quickly for strain rates below $10^{-5}/\text{s}$, indicating a shift of deformation behavior from grain interior plasticity to GB creep. (b) The relationship between flow stress and strain rates from experiments on nc Cu with an average grain size of $d=30\text{nm}$ and the present model for different grain sizes. The calculations show a transition from diffusion and sliding controlled steady-state creep at low strain rates to dislocation controlled plastic deformation at high strain rates. At the low end of strain rates, there is a linear relationship between strain rates and flow stresses. At the high end of strain rates, the flow stress becomes increasingly independent of strain rates.

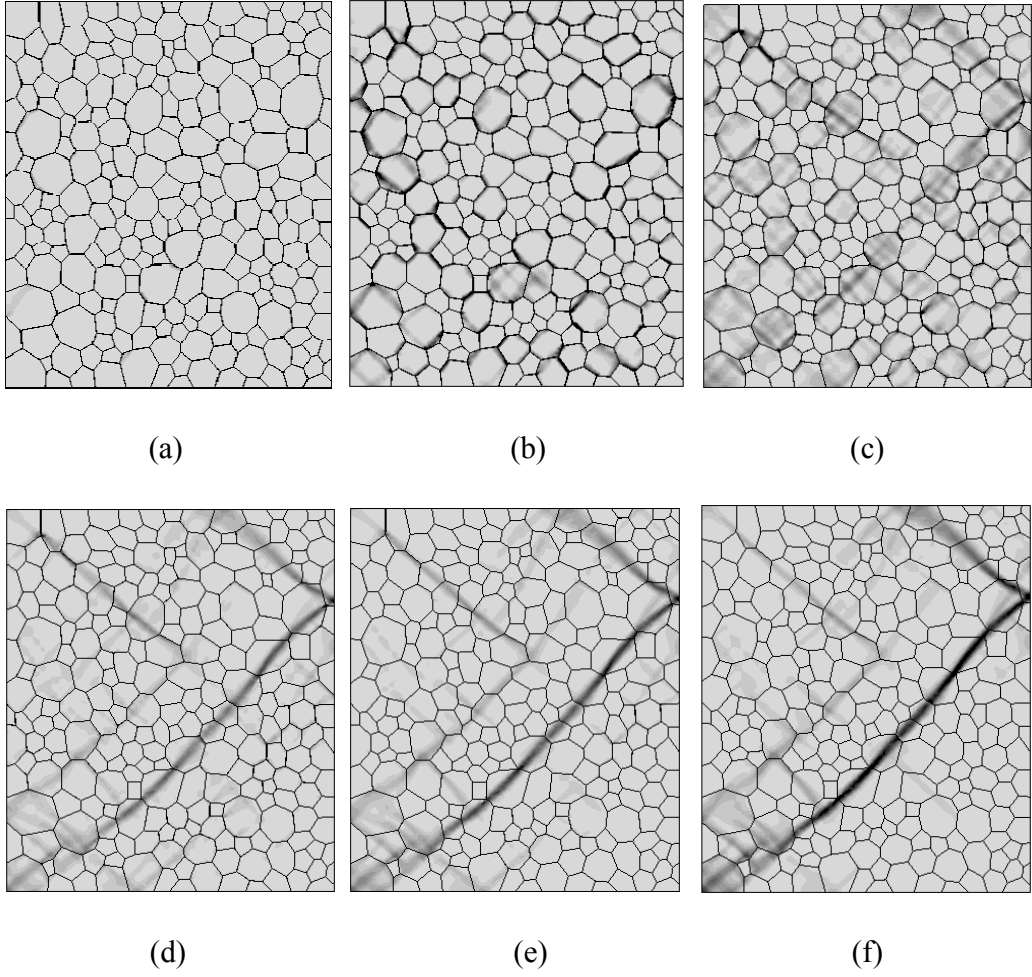
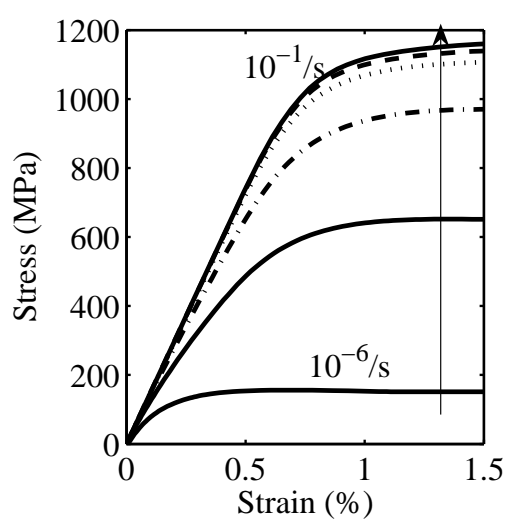
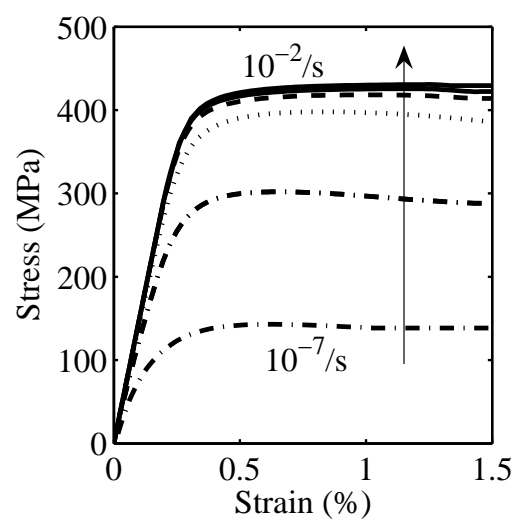


Fig. 6. Equivalent plastic deformation in grain interior at a macroscopic strain of 1.5% for different strain rates ($\bar{\varepsilon}^p=0.15$ in the black region and $\bar{\varepsilon}^p=0.0$ in the lightest region): (a) $\dot{\varepsilon}=10^{-6}/s$; (b) $\dot{\varepsilon}=10^{-5}/s$; (c) $\dot{\varepsilon}=10^{-4}/s$; (d) $\dot{\varepsilon}=10^{-2}/s$; (e) $\dot{\varepsilon}=10^{-1}/s$; (f) $\dot{\varepsilon}=10^2/s$. As the strain rate increases, plastic deformation undergoes three typical stages: (I) for strain rates below $10^{-6}/s$, deformation occurs primarily by GB diffusion and sliding; (b) for intermediate strain rates between $10^{-6}/s$ and $10^{-4}/s$, both GB creep and grain interior plasticity contribute to deformation. (c) for strain rates above $10^{-2}/s$, dislocation controlled plasticity in grain interiors dominates and leads to shear band type of failure.



(a)



(b)

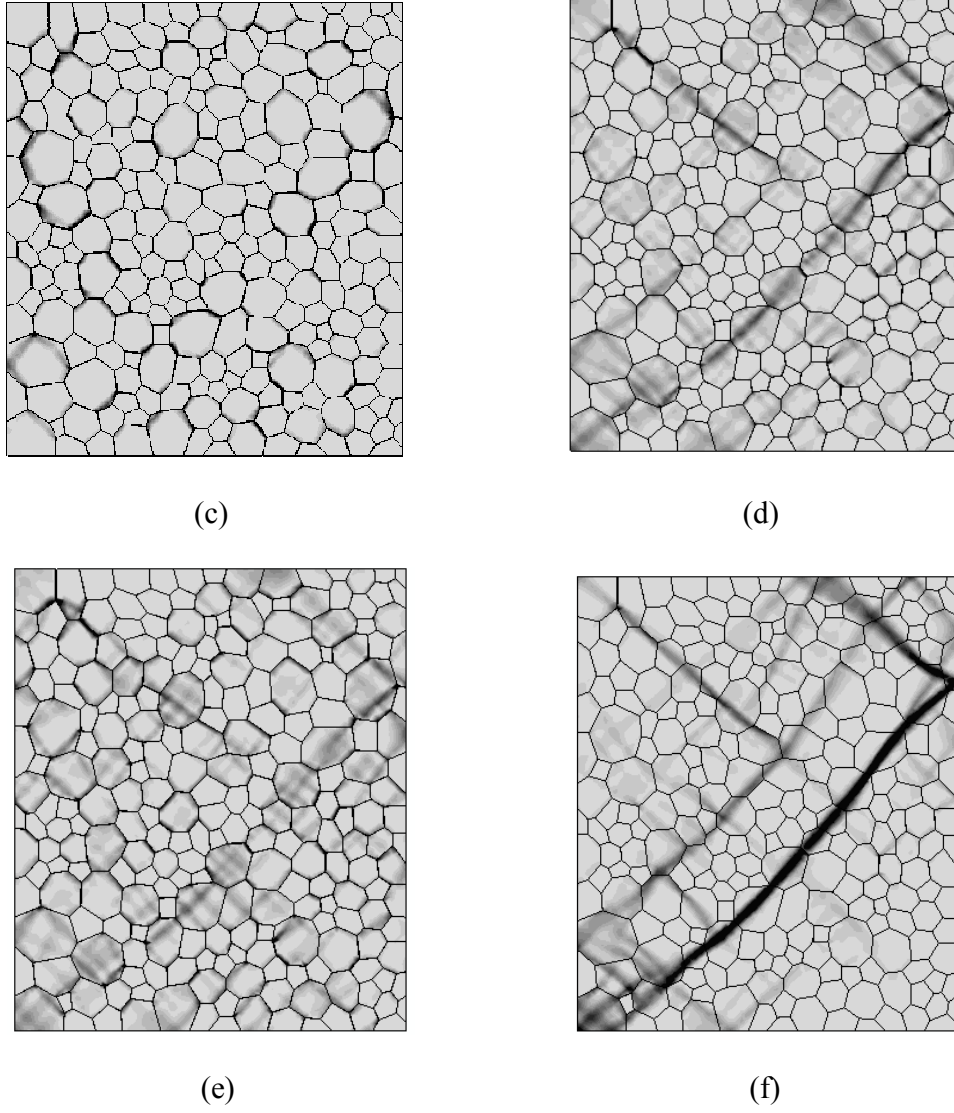


Fig. 7. Mechanical behavior of nc Cu with an average grain size of 20nm and 50nm ($\bar{\epsilon}^p=0.15$ in the black region and $\bar{\epsilon}^p=0.0$ in the lightest region). (a) and (b) Stress-strain curves at different strain-rates for $d=20\text{nm}$ and 50nm , respectively. Equivalent plastic strain in grain interior at a macroscopic strain of 1.5% under different structure and loading conditions: (c) $d=20\text{nm}$ and $\dot{\epsilon}=10^{-5}/\text{s}$; (d) $d=20\text{nm}$ and $\dot{\epsilon}=10^{-3}/\text{s}$; (e) $d=50\text{nm}$; and $\dot{\epsilon}=10^{-5}/\text{s}$; (f) $d=50\text{nm}$ and $\dot{\epsilon}=10^{-3}/\text{s}$.

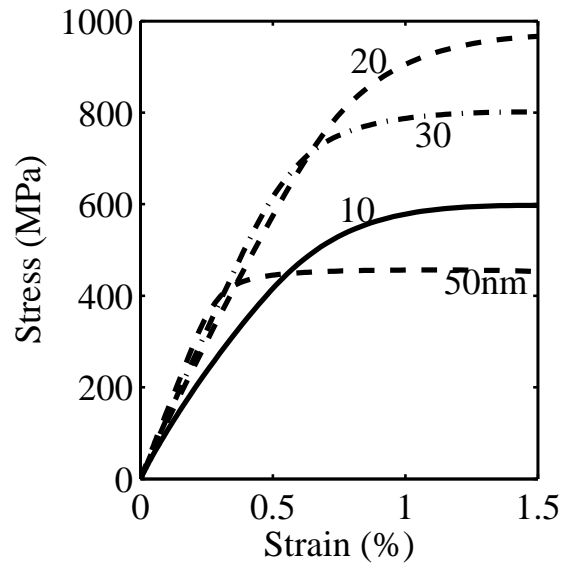


Fig. 8. Softening in strength as grain sizes decreases. Stress-strain curves for different grain sizes at a fixed strain rate of 10^{-4} /s. Softening is primarily due to increasing GB deformation.

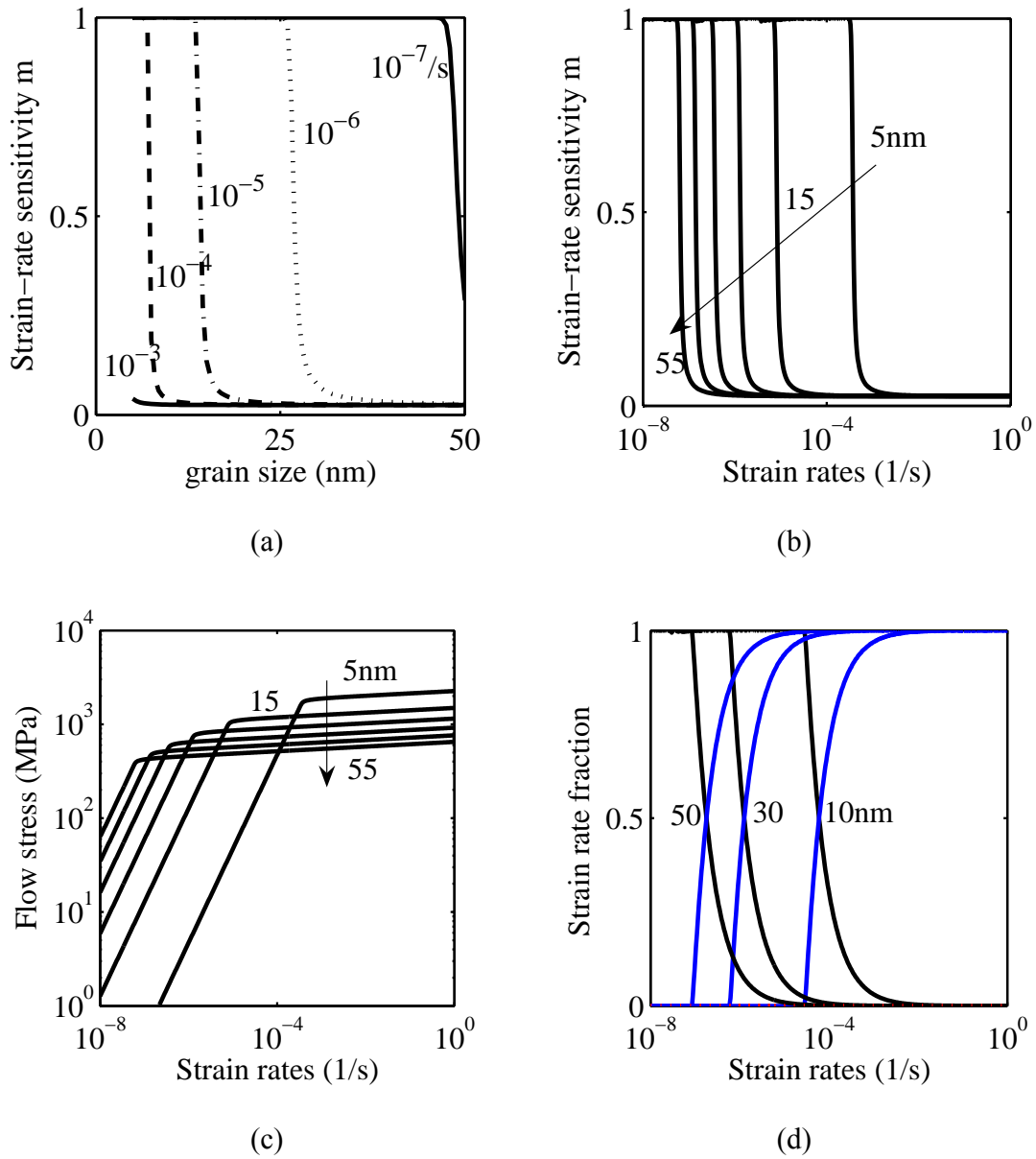


Fig. 9. Model prediction of strain-rate sensitivity and flow stress versus strain rate and grain size. (a) The strain-rate sensitivity m as a function of grain size at different strain rates. It increases quickly as the grain size decreases. (b) The strain-rate sensitivity m as a function of strain rate at different grain sizes. It increases quickly with strain rates below a grain-size dependent critical value, indicating a shift of deformation behavior from grain interior plasticity to GB creep. (c) The steady-state flow stress as a function of the strain rate for different grain sizes shows clearly the transition from GB dominated deformation to that controlled by grain interior plasticity. (d) The strain rate fractions versus strain rates at different grain sizes. The black curves are contributions from GB diffusion, and blue curves are those for grain plasticity via complete dislocation motion; and red curves (at the bottom) are contributions by partial dislocation activities, which is negligible.

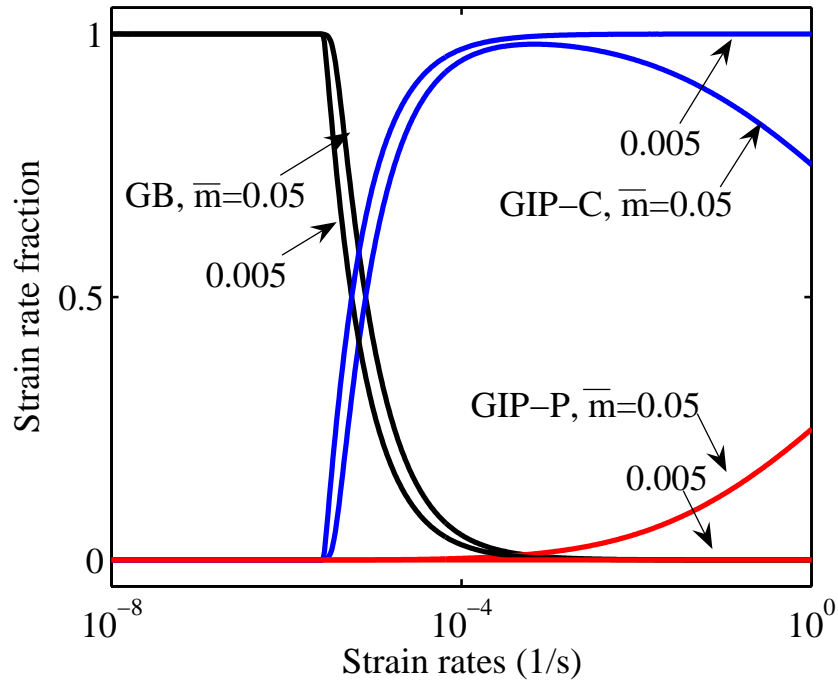


Fig. 10. Model predictions on the influence of strain-rate sensitivity in grains to the deformation in grain-boundaries (GB), grain-interior plasticity by complete dislocations (GIP-C) and that by partial dislocations (GIP-P) for a sample with average grain size of $d=20\text{nm}$. The strain-rate fraction by GB is 1 at extremely low strain rates and zero at sufficiently high strain rates; for intermediate strain rates, it decreases with increasing strain rates. Increasing \bar{m} slightly speeds up the transition. The contribution from GIP-P is negligible in the low strain rate regime, and becomes conceivable to significant in the high strain rate regime as \bar{m} increases. The strain-rate fraction for GIP-C increases monotonically with increasing strain rates when \bar{m} is close to zero. For relatively large \bar{m} , its contribution increases with strain rates in the low strain rate regime, reaches a maximum and then starts to decrease with further increase of strain rates.